Journal of Superconductivity and Novel Magnetism (2022) 35:1261–1268
https://doi.org/10.1007/s10948-022-06190-z

ORIGINAL PAPER

Microstructure, Magnetic Properties, and Thermal Stability of Bulk Anisotropic $SmCo_7$/α-Fe(Co) + $Nd_2Fe_{14}B$/α-Fe Multiphase Nanohybrid Magnets

Yana Wang[1,2] · Wenpeng Song[1,2] · Guangwei Huang[1,2]

Received: 13 November 2021 / Accepted: 18 December 2021 / Published online: 24 February 2022

Abstract
In this report, we have fabricated anisotropic bulk $SmCo_7$/α-Fe(Co) + $Nd_2Fe_{14}B$/α-Fe multiphase nanohybrid magnets using high-pressure thermal compression deformation of the mixtures of $Nd_9Fe_{83.2}Ti_{0.8}Nb_1B_6$ amorphous-nanocrystalline powder and SmCo-based amorphous-nanocrystalline powder. The microstructure, magnetic properties, and thermal stability of the multiphase nanohybrid magnet were researched. The obtained magnet features a high energy product of 22.5 MGOe at room temperature on basis of the microstructure with a (00 *l*) $SmCo_7$ hard magnetic phase texture and small nanograin sizes for all components. An energy product of 14.8 MGOe has been obtained at 200 °C due to the magnet possessing a small $\beta_{(RT\text{-}250\,^{\circ}C)} = -0.25\%\ ^{\circ}C^{-1}$. Moreover, the magnet with a good thermal stability of nanostructure has also been studied. This work shows that the bulk anisotropic $SmCo_7$/α-Fe(Co) + $Nd_2Fe_{14}B$/α-Fe multiphase nanohybrid magnets have a high potential for high-temperature applications. Meanwhile, this work gives a method of further improving the thermal stability of the multiphase nanohybrid magnets.

Keywords Nanohybrid magnets · Anisotropy · Thermal stability · High-temperature properties

1 Introduction

Permanent magnetic materials including no heavy rare earths (Dy or Tb), low cost, and capable of operating at elevated temperatures (≥ 200 °C) are needed for applications in advanced power systems such as motors, hybrid vehicles, and wind generators [1–3]. Sm-Co and Nd-Fe-B rare-earth permanent magnets are preferred materials in these systems because these magnets have high energy products (> 20 MGOe), which can satisfy the weight or size limitation of these systems [4, 5]. However, the Nd-Fe-B-based magnet presents poor high-temperature magnetic properties resulting from their low Curie temperature (312 °C) and large negative thermal coefficients for coercivity β and remanence α, and hence, the addition of significant amounts of heavy rare-earth elements Dy or Tb is needed to increase the thermal stability of the Nd-Fe-B-based magnets [6, 7]. Unfortunately, Dy and Tb are essential elements on basis of supply risk and the importance of clean energy [8]. In contrast, the Sm-Co-based magnets have excellent thermal stability in the upper temperature range due to their high Curie temperatures (from 680 to 920 °C) and a large magnetocrystalline anisotropy [9], but their energy product is below that of the Nd-Fe-B-based magnet at room temperature (RT) resulting from their rather low saturation magnetization [10]. Furthermore, the rare-earth permanent magnet supplies have aroused extensive attention in recent years. It is ascribed to that the rare-earth permanent magnets hold the key to improving the efficiency and property of equipment in power generation, conversion, transportation, and other economic energy-use areas [11]. These phenomena have promoted the lean rare earth or non-rare-earth magnets becoming an investigation hotspot in the sector of permanent magnetic materials [12–14].

Nowadays, nanohybrid magnets composed of hard magnetic phases featuring high coercivity and soft magnetic phases featuring high saturation magnetization at nanoscale

✉ Guangwei Huang
huang35168@sina.com

[1] Hebei Engineering Research Centre for Rare Earth Permanent Magnetic Materials & Applications, Hebei University of Engineering, Handan 056038, China

[2] College of Materials Science and Engineering, Hebei University of Engineering, Handan 056038, China

aroused broad attention because they were expected to become a new type of strong magnet with less rare-earth metal content [12, 15–21]. Recently, we have succeeded in yielding bulk anisotropic $SmCo_7$/α-Fe(Co) + $Nd_2Fe_{14}B$/α-Fe multiphase nanohybrid magnets with high energy product (25 MGOe) and high-content soft phases (~ 30 wt%) [22]. Moreover, these magnets possess a good thermal stability ($\beta_{(RT\text{-}250\ ^\circ C)} = -0.28\%\ ^\circ C^{-1}$) resulting from the synergetic effect exerted by the soft-phase α-Fe and α-Fe(Co), and the hard-phase $Nd_2Fe_{14}B$ and $SmCo_7$ [22]. On basis of the discoveries, the bulk $SmCo_7$/α-Fe(Co) + $Nd_2Fe_{14}B$/α-Fe multiphase nanohybrid magnets, having high magnetic properties and low cost, feature great practical application potential; thus, it is very necessary to further investigate this type of multiphase nanohybrid magnet.

We all know that the composition and structure of materials significantly affect the physical and chemical performances of materials [4, 6, 23, 24]. Hence, changing the composition or structure of the precursors is an alternative approach to produce the bulk $SmCo_7$/α-Fe(Co) + $Nd_2Fe_{14}B$/α-Fe multiphase nanohybrid magnets with optimized magnetic performance. Here, we focus on fabricating the bulk $SmCo_7$/α-Fe(Co) + $Nd_2Fe_{14}B$/α-Fe multiphase nanohybrid magnet by high-pressure thermal compression (HPTC) deformation of the mixtures of $Nd_9Fe_{83.2}Ti_{0.8}Nb_1B_6$ amorphous-nanocrystalline powder and SmCo-based amorphous-nanocrystalline powder precursor. Precursors used in this work are different from previous studies. In the previous work, the precursors were the mixture of $Nd_9Fe_{85.5}Cu_{1.5}B_4$ amorphous powder and SmCo-based amorphous-nanocrystal powder [22]. The microstructure, magnetic performances, and thermal stability of the magnets yielded from HPTC deformation of the precursors were studied in this investigation. We find that the bulk anisotropic $SmCo_7$/α-Fe(Co) + $Nd_2Fe_{14}B$/α-Fe multiphase nanohybrid magnet exhibits an energy product of 22.5 MGOe at RT and 14.8 MGOe at 200 °C under the microstructure with a (00 *l*) texture of $SmCo_7$ phase and fine nanograin sizes for all components. Moreover, these obtained magnets display a good thermal stability with a small $\beta_{(RT\text{-}250\ ^\circ C)} = -0.25\%\ ^\circ C^{-1}$ and a good thermal stability of nanostructure. Resultants exhibit obtained magnets feature high high-temperature applications potential.

2 Experimental

In this investigation, the HPTC precursors were consisted of $Nd_9Fe_{83.2}Ti_{0.8}Nb_1B_6$ amorphous-nanocrystalline powder and SmCo-based amorphous-nanocrystalline powder. To gain $Nd_9Fe_{83.2}Ti_{0.8}Nb_1B_6$ amorphous-nanocrystalline powder, the $Nd_9Fe_{83.2}Ti_{0.8}Nb_1B_6$ alloy ingot was fabricated through arc melting in an argon atmosphere employing industrial pure Nd, Ti, Nb, and Fe metals and Fe_3B alloy, firstly. Then, the alloy ingots were adopted for preparing ribbons through melt spinning at a tangential speed of 26 m/s. Finally, the ribbons were milled into amorphous-nanocrystalline powder applying a high-energy mill (SPEX 8000 M) in an Ar atmosphere. The weight ratio of the specimen to the ball was 1:20 and the milling time was 1.5 h (h). For obtaining the SmCo-based amorphous-nanocrystalline powders, industrial $SmCo_5$ (powder size ~ 40 m), Fe (powder size < 5 m), and Co (powder size < 5 m) materials were blended and subjected to high-energy ball milling, where the milling time was 4 h and the sample-to-ball weight ratio was 1:20. In $SmCo_5$ + FeCo (a weight ratio of Fe and Co was 65:35) abrasive material, the weight fraction of FeCo load was 30%. The HPTC precursors were the blends of the $Nd_9Fe_{83.2}Ti_{0.8}Nb_1B_6$ amorphous-nanocrystalline and SmCo-based amorphous-nanocrystal powder with a weight ratio of 30:70. The precursor was then consolidated into a bulk cylinder with a relative density of 80% in an Ar atmosphere at RT. The bulk specimens were placed in a steel tube and the HPTC deformation was performed on the specimen unit in vacuum adopting Gleeble 3800 machine. The HPTC deformation process is as follows: deformation temperature $T = 700$ °C, deformation time $t = 30$ s (s), height reduction (strain) = 79%, and maximal stress $\sigma = 700$ MPa. The disc-shaped HPTC-deformed specimen with a mean diameter of about 15 mm and a thickness of about 1.2 mm were generated, and the specimen density was detected to be $\rho = 8.2$ g/cm^3 by Archimedes' principle.

Transmission electron microscopy (TEM) and X-ray diffraction (XRD) with Co K_α radiation were employed for characterizing the microstructure of the HPTC-deformed specimens. The volume fraction and grain size of the nanocrystals were detected from the determined XRD pattern employing the Rietveld refinement program via the HighScore Plus software, where the goodness of fitting < 2, a profile R-value $R_p < 10$, and a weighted profile R-value $R_{wp} < 10$ were acquired. The RT and high-temperature magnetic properties of HPTC-deformed specimens were determined employing a vibrating specimen magnetometer (VSM) with a maximal magnetic field of 21 kOe, where the demagnetization effect was corrected by traditional methods [18]. Thermal stability was characterized through temperature coefficients of remanence α and coercivity β just as many reported works [24, 25].

3 Results and Discussion

3.1 Structural Analyses

Figure 1 exhibits the XRD pattern of HPTC-deformed magnet precursors. XRD analyses prove the precursors are blends of

$Nd_9Fe_{83.2}Ti_{0.8}Nb_1B_6$ amorphous-nanocrystalline powder and SmCo-based amorphous-nanocrystalline powder (Fig. 1c). The $Nd_9Fe_{83.2}Ti_{0.8}Nb_1B_6$ amorphous-nanocrystalline powder is a blend of amorphous and crystal phases of α-Fe with a grain size of 5–7 nm (Fig. 1a), and the SmCo-based amorphous-nanocrystalline powder is a blend of amorphous and crystalline phases of α-Fe(Co) with a grain size of 5–7 nm (Fig. 1b). Therefore, the precursors for the HPTC-deformed magnets are a blend of amorphous and crystal phases of α-Fe and α-Fe(Co) with a fine nanograin size (Fig. 1c). These results indicate that the precursors in this work are different form that in Ref. 22.

Figure 2 displays the XRD patterns of HPTC-deformed magnets determined on the specimen surface perpendicular to the pressure direction. XRD analyses prove the HPTC-deformed magnets comprise $SmCo_7$, $Nd_2Fe_{14}B$, α-Fe(Co), and α-Fe crystalline phases (Fig. 2a), as described in the previous work [22]. In further analyses of the XRD spectrum, weight fractions of $SmCo_7$, α-Fe(Co), $Nd_2Fe_{14}B$, and α-Fe phases are determined as about 56%, 14%, 24%, and 6%, respectively, and the mean grain sizes of $SmCo_7$, $Nd_2Fe_{14}B$, α-Fe(Co), and α-Fe phases are determined as about 12 nm, 15 nm, 13 nm, and 13 nm, separately. These outcomes prove the HPTC-deformed magnet majorly contains four crystal phases, namely, $SmCo_7$ and $Nd_2Fe_{14}B$ hard magnetic phases and α-Fe(Co) and α-Fe soft magnetic phases. Resultants show that the $SmCo_7$ and $Nd_2Fe_{14}B$ hard magnetic phases for the HPTC-deformed magnets come from the amorphous matrix in the HPTC process. We conclude that the multiphase nanohybrid magnet is produced by HPTC deformation of blends of $Nd_9Fe_{83.2}Ti_{0.8}Nb_1B_6$ amorphous-nanocrystalline powder and the SmCo-based amorphous-nanocrystalline powder.

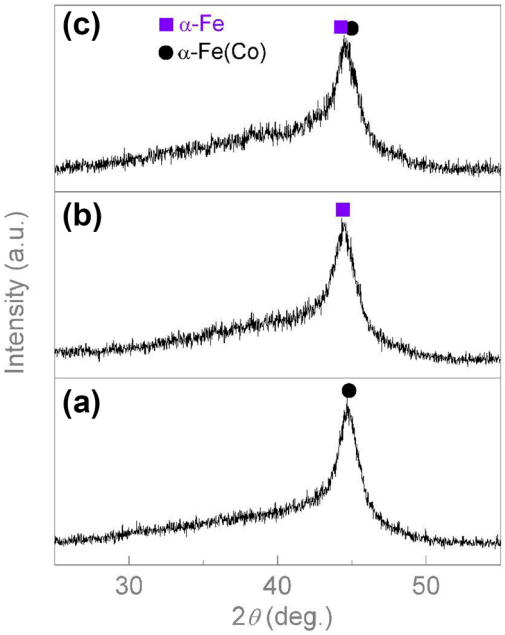

Fig. 1 XRD patterns of the as-milled $Nd_9Fe_{83.2}Ti_{0.8}Nb_1B_6$ amorphous-nanocrystalline powders (**a**), as-milled SmCo-based amorphous-nanocrystalline powder (**b**), and blends of as-milled $Nd_9Fe_{83.2}Ti_{0.8}Nb_1B_6$ amorphous-nanocrystalline powder and SmCo-based amorphous-nanocrystalline powder (**c**)

Through further detailed analyses of XRD patterns, we discovered that, for the HPTC-deformed magnet, the $SmCo_7$ hard-phase nanocrystals possess a (00 *l*) texture along the pressure direction (Fig. 2a, c). $SmCo_7$ nanocrystal texture is expressed by the improved intensity of (002) diffraction peak, where the ratio of $I_{(002)}/I_{(111)} = 64\%$ exceeds that $I_{(002)}/I_{(111)} = 30\%$ of isotropic $SmCo_7$ crystals (see the Inorganic Crystal Structure Database ICSD:168,273). However, the (00 *l*) texture of $Nd_2Fe_{14}B$ hard-phase nanocrystals cannot be found, which is indicated by the $I_{(004)}/I_{(220)} = 71\%$ is similar to that $I_{(004)}/I_{(220)} = 70\%$ of isotropic $Nd_2Fe_{14}B$ crystals (see ICSD:067,224) (Fig. 2a, b). These results demonstrate that the bulk anisotropic $SmCo_7$/α-Fe(Co) + $Nd_2Fe_{14}B$/α-Fe multiphase nanohybrid magnet can be prepared by HPTC technology, even though the HPTC-deformed magnets only exhibit the (00 *l*) texture of $SmCo_7$ hard-phase nanocrystals, and the $Nd_2Fe_{14}B$ hard-phase nanocrystals do not display the (00 *l*) texture.

TEM observations were employed for further characterizing the morphology of the HPTC-deformed magnets. Figure 3a shows that the HPTC-deformed magnets are composed of two regions, which are determined to be $SmCo_7$/α-Fe(Co) and $Nd_2Fe_{14}B$/α-Fe regions, separately. In the $SmCo_7$/α-Fe(Co) regions (Fig. 3b), the microstructure comprises approximately equiaxed $SmCo_7$ and α-Fe(Co) nanocrystals featuring a mean grain size of about 12 nm (inset of Fig. 3b). The $SmCo_7$ nanocrystals display a (00 *l*) texture along the direction of pressure, implied by stronger (002) diffraction points in the selected region electron diffraction (SAED) pattern (inset of Fig. 3b). These results coincide with the XRD studies. In the $Nd_2Fe_{14}B$/α-Fe regions (Fig. 3c), the microstructure consists of approximately equiaxed α-Fe and $Nd_2Fe_{14}B$ nanocrystals featuring a mean grain size of ~ 15 nm (inset of Fig. 3c). The $Nd_2Fe_{14}B$ nanocrystals show arbitrary orientation, which is indicated by the SAED pattern (inset of Fig. 3c) in keeping with XRD resultants. These findings prove the HPTC-deformed magnet possesses a (00 *l*) texture of $SmCo_7$ hard magnetic nanocrystals and small nanograin sizes for all components.

$SmCo_7$ hard magnetic nanocrystals are oriented along their easy magnetizing direction in obtained magnets. It results from the preferential nucleation and growth of $SmCo_7$ nanocrystals from SmCo amorphous matrix under the HPTC process, which introduces strain-energy anisotropy, facilitating the directional nucleation and growth of nanocrystals along the minimal strain-energy direction [16–18, 26, 27]. By contrast, the $Nd_2Fe_{14}B$ hard magnetic nanocrystals do

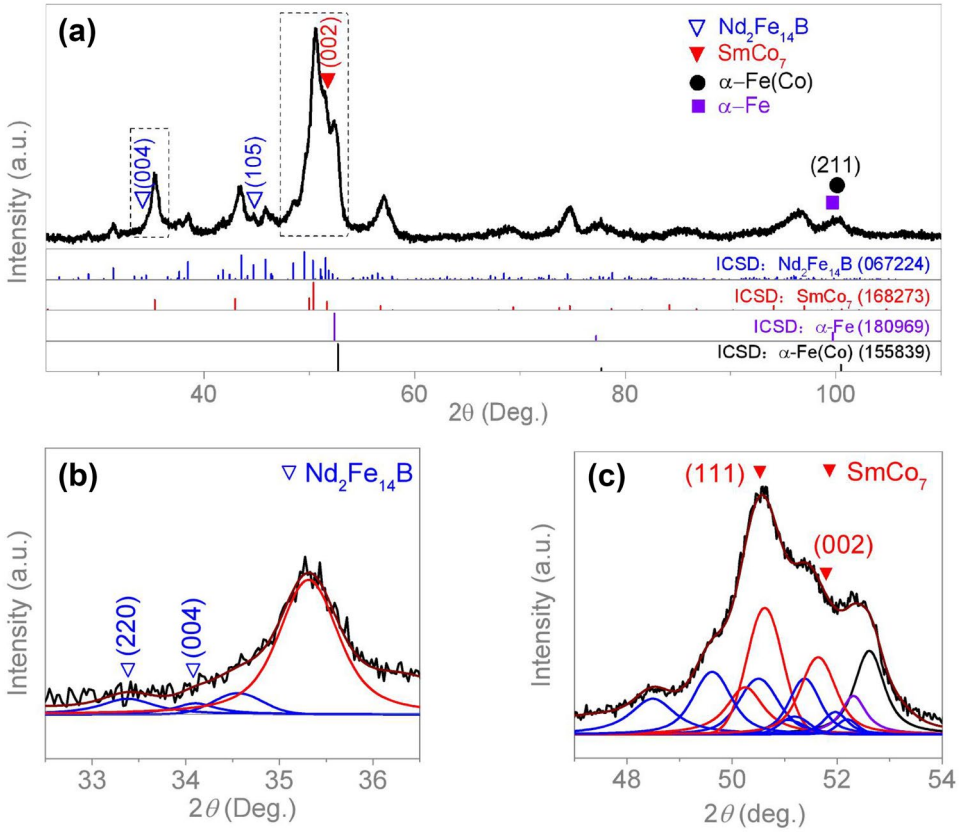

Fig. 2 XRD patterns of the HPTC-deformed bulk $SmCo_7$/α-Fe(Co)+$Nd_2Fe_{14}B$/α-Fe multiphase nanohybrid magnets determined on the specimen surface perpendicular to the pressure direction (**a**). The vertical lines imply powder diffraction data of isotropic $Nd_2Fe_{14}B$, $SmCo_7$, α-Fe, and α-Fe(Co) crystals. (**b**, **c**) The magnified view of the XRD pattern in plane (**a**). Individual XRD peaks isolated from the pattern employing the PeakFit software

not have any orientation, which is different from those previous studies [17, 22, 27, 28]. This result mainly ascribes to that the material composition and microstructure of Nd-Fe-B precursors are different from those reported work's precursors [17, 22, 27, 28]. A further deep study for this phenomenon will be conducted in the future research work. Based on the XRD measurements and the TEM analyses, small grain sizes of nanocrystals for each component were realized in the HPTC-deformed magnets. The small grain sizes result from the dispersion of ultrafine α-Fe(Co) and α-Fe nanograins (5–7 nm) in an amorphous matrix before HPTC deformation and rapid deformation time (~ 30 s) during HPTC deformation process, as demonstrated in previous studies [16–18, 22].

3.2 Magnetic Properties

After characterizing synthesized nanohybrid magnets, we investigated the magnetic properties of the HPTC-deformed magnet. The magnet presents obvious magnetic anisotropy with $4\pi M_r^{\parallel}/4\pi M_r^{\perp} = 1.26$ (Table 1), which is further demonstrated by the easy-axis and hard-axis magnetic behavior parallel and perpendicular to the pressure direction (Fig. 4). For the HPTC-deformed magnet along the pressure direction at RT, the maximum energy product of $(BH)_{max} = 22.5$ MGOe was obtained (Table 1). This $(BH)_{max}$ comes from the high remanence ratio $4\pi M_r/4\pi M_s = 0.87$ and coercivity $H_{ci} = 4.4$ kOe (Table 1), where $4\pi M_r$ and $4\pi M_s$ represent the remanence and saturation magnetization along the pressure direction, respectively. The high value of $4\pi M_r/4\pi M_s = 0.87$ along easy axis comes from the (00 *l*) texture of $SmCo_7$ nanocrystalline and excellent exchange coupling between small nanocrystalline, where the exchange coupling occurs between small nanocrystalline of α-Fe(Co) and $SmCo_7$ as well as between the small $Nd_2Fe_{14}B$ and α-Fe nanocrystals [29–31]. The $H_{ci} = 4.4$ kOe comes from the synergetic effect exerted by $SmCo_7$ and $Nd_2Fe_{14}B$ nanocrystals as well as the pinning-type coercivity mechanisms in nanostructured permanent magnets [32–34]. Besides, we believe the interfaces between $SmCo_7$/α-Fe(Co) regions and $Nd_2Fe_{14}B$/α-Fe regions significantly affect magnetic performances of this kind of multiphase nanohybrid magnet, and we will carry out such studies in the future work.

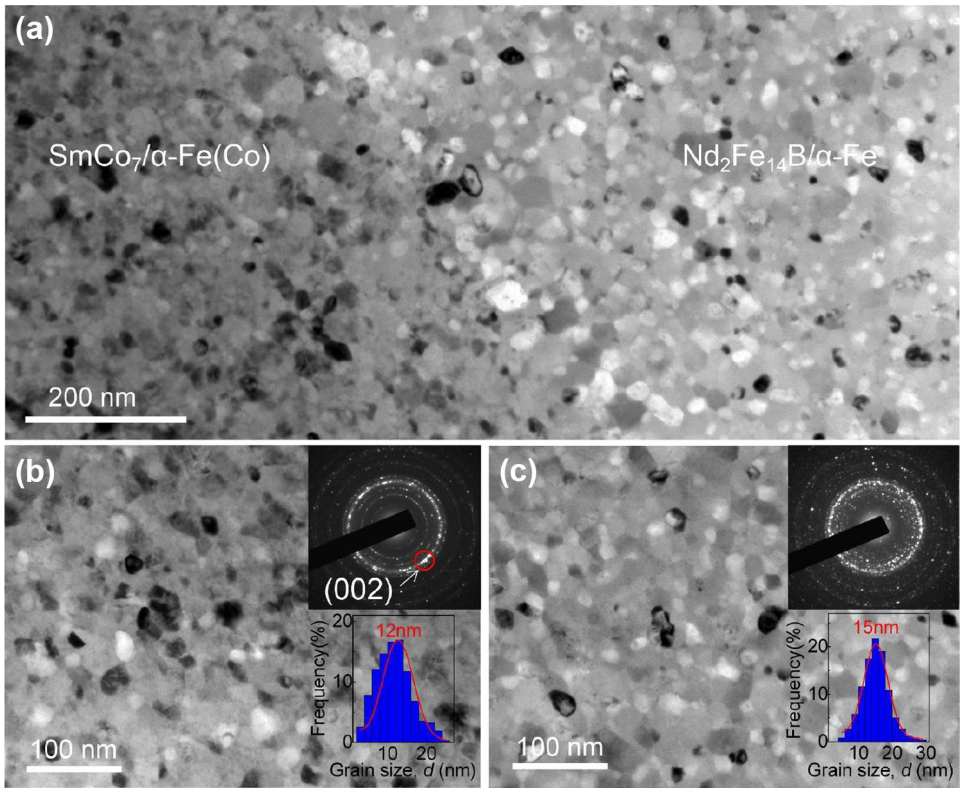

Fig. 3 Characterization of synthesized bulk $SmCo_7$/α-Fe(Co) + $Nd_2Fe_{14}B$/α-Fe multiphase nanohybrid magnets produced through HPTC. (**a**) The bright-field TEM image of the magnet including the $SmCo_7$/α-Fe(Co) region and the $Nd_2Fe_{14}B$/α-Fe region. (**b**) The bright-field image of the $SmCo_7$/α-Fe(Co) region and corresponding SAED pattern and statistic distribution of the nanograin size (insets). (**c**) The bright-field image of the $Nd_2Fe_{14}B$/α-Fe region and corresponding SAED pattern and statistic distribution of the nanograin size (insets). TEM images were determined on the specimen surface parallel to the pressure direction

Figure 5 exhibits the demagnetizing curves for HPTC-deformed magnets measured along the pressure direction at different high temperatures. It is suggested that the magnets present good single-phase magnetic behavior at the different high temperatures and the energy product of 14.8 MGOe is achieved at 200 °C (Figs. 5 and 6). The thermal stability of the HPTC-deformed magnet was investigated by measuring its remanence () and coercivity () temperature coefficients [24, 25]. The HPTC-deformed magnets exhibit a low $_{(\text{RT-250 °C})} = -0.02\%\ °C^{-1}$ and $\beta_{(\text{RT-250 °C})} = -0.25\%\ °C^{-1}$. The $\beta_{(\text{RT-250 °C})} = -0.25\%\ °C^{-1}$ (Fig. 6) is less than $\beta_{(\text{RT-250 °C})} = -0.26\%\ °C^{-1}$, $\beta_{(\text{RT-250 °C})} = -0.42\%\ °C^{-1}$ or $\beta_{(\text{RT-250 °C})} = -0.4\%\ °C^{-1}$ for single-phase $SmCo_5$, Nd-Fe-B or Nd-Dy-Fe-Co-B magnet, respectively [1, 35]. In particular, the $\beta_{(\text{RT-250 °C})} = -0.25\%\ °C^{-1}$ in this investigation is smaller than the values of $-0.28\%\ °C^{-1}$ and $-0.3\%\ °C^{-1}$ for our previous works [22, 36]. It is mainly contributed to that the $Nd_2Fe_{14}B$/α-Fe regions have a small grain size and $Nd_2Fe_{14}B$ phase contains Ti and Nb elements [37, 38]. These results demonstrate that changing the precursors for the HPTC-deformed magnets can further improve the temperature stability of the multiphase nanohybrid magnets.

The thermal stability of nanostructure for the nanostructure materials is of great importance for their practical applications. For studying the thermal stability of HPTC-deformed magnet nanostructures, the $(BH)_{max}$

Table 1 Magnetic properties of bulk $SmCo_7$/α-Fe(Co) + $Nd_2Fe_{14}B$/α-Fe multiphase nanohybrid magnets produced through HPTC. These magnetic properties came from the hysteresis loop given in Fig. 4

HPTC magnet	$(BH)_{max}$ (MGOe)	H_{ci} (kOe)	B_r (kG) ($B = H + 4\pi M$)	M_s (kG)	S	$4\pi M_r^{\parallel}/4\pi M_r^{\perp}$
$\parallel P$	22.5	4.4	11.67	13.35	0.87	1.26
$\perp P$	9.8	4.25	9.24	12.53	0.74	

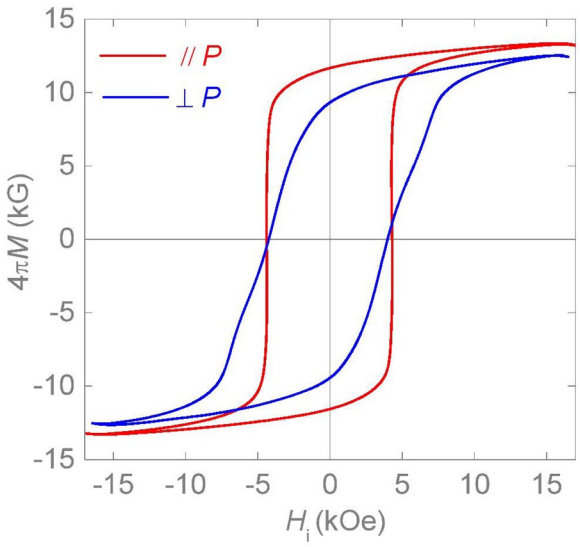

Fig. 4 Hysteresis loops of the bulk $SmCo_7$/α-Fe(Co) + $Nd_2Fe_{14}B$/α-Fe multiphase nanohybrid magnet measured parallel (∥) and perpendicular (⊥) to the pressure (P) direction at RT

along the pressure direction was obtained at RT after long-run annealing at $T_a = 400$ °C in a vacuum chamber at $p < 10^{-4}$ Pa (Fig. 7a). These values of $(BH)_{max}$ are no degradation after annealing at different times at $T_a = 400$ °C, and thus suggesting the HPTC-ed magnet with a stable nanostructure morphology. This result has been further verified by Fig. 7b, which shows a rigorous single-phase demagnetization behavior after being heat treatment. These results demonstrate the HPTC-deformed magnet possesses a stable nanostructure for the potential applications.

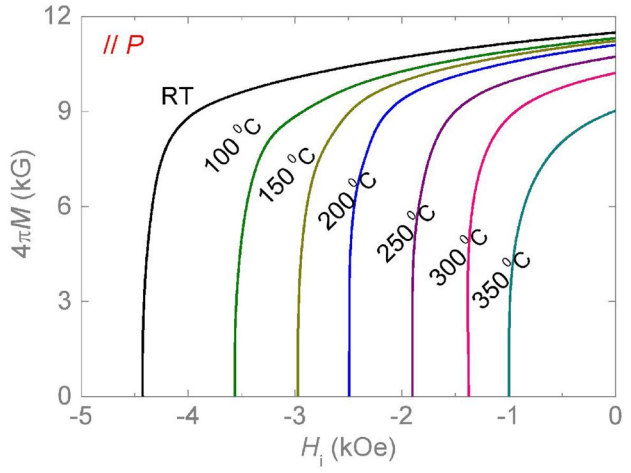

Fig. 5 Demagnetization curves for the HPTC-deformed magnets measured along the direction of pressure at different high temperatures

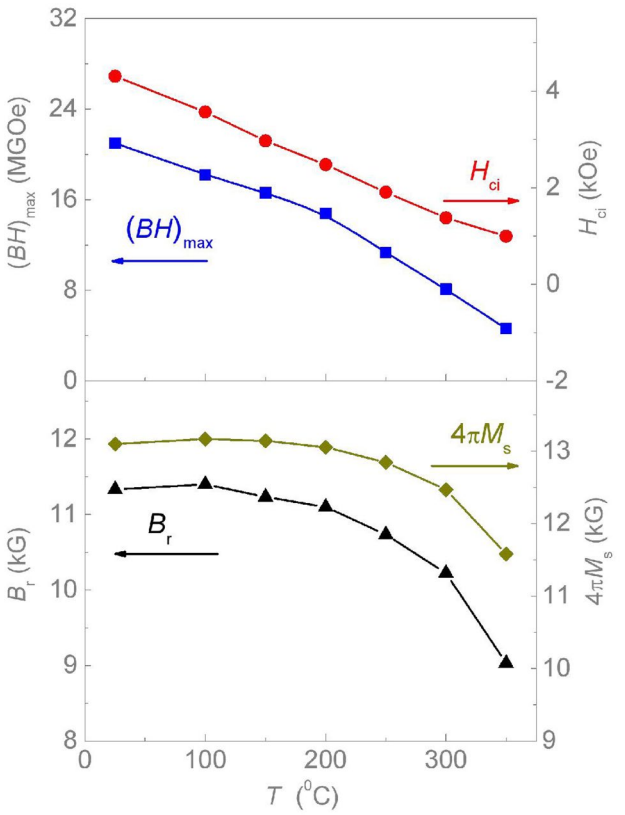

Fig. 6 Dependence of $(BH)_{max}$, H_{ci}, B_r, and $4\pi M_s$ on the measurement temperatures for the HPTC-deformed magnets measured along the direction of pressure. These magnetic properties came from the hysteresis loop given in Fig. 5

3.3 Discussion

The anisotropic bulk $SmCo_7$/α-Fe(Co) + $Nd_2Fe_{14}B$/α-Fe magnets featuring an improved thermal stability and good magnetic properties were fabricated with HPTC technology. However, the maximum energy product (22.5 MGOe) for the HPTC-deformed magnet is still low as compared with the sintered and hot deformed single-phase magnets such as $SmCo_5$, Sm_2Co_{17}, and $Nd_2Fe_{14}B$ magnets. In order to promote the practical applications of multiphase nanohybrid magnets, enhanced energy product is of great significance for the bulk $SmCo_7$/α-Fe(Co) + $Nd_2Fe_{14}B$/α-Fe multiphase nanohybrid magnets. For enhancing the maximum energy product for the HPTC-deformed magnet, it is necessary to further enhance the B_r and the H_{ci} for the obtained magnets simultaneously. Many previous studies show that further aligning hard-phase nanograins and engineering their interface structure could be further enhanced the B_r and the H_{ci}, thus promoting the synthesized magnets having enhanced energy products [39–41]. Therefore, higher energy products for the $SmCo_7$/α-Fe(Co) + $Nd_2Fe_{14}B$/α-Fe multiphase nanohybrid magnets could be achieved by further enhancing the

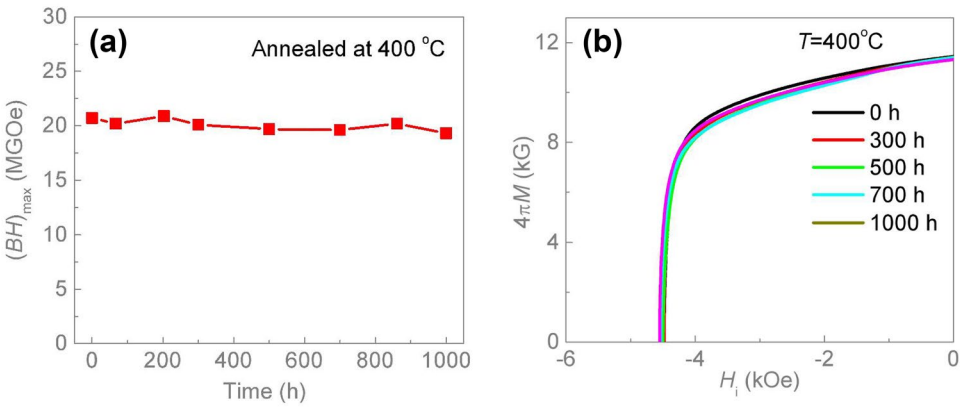

Fig. 7 (**a**) $(BH)_{max}$ and (**b**) demagnetizing curves along the pressure direction measured at RT after different annealing times at $T_a = 400$ °C

hard-phase texture along the easy direction of magnetization and adjusting the interface structure between nanocrystals or the different regions.

4 Conclusions

Bulk anisotropic $SmCo_7$/α-Fe(Co) + $Nd_2Fe_{14}B$/α-Fe multiphase nanohybrid magnets were prepared using HPTC technique. The microstructure, magnetic properties, and thermal stability of HPTC-deformed magnets have been investigated. We discovered HPTC-deformed magnets with a low $\beta_{(RT\text{-}250\ ^\circ C)} = -0.25\%\ ^\circ C^{-1}$ exhibit a maximal energy product of 22.5 MGOe at RT and 14.8 MGOe at 200 °C. This work shows that the HPTC-deformed bulk anisotropic $SmCo_7$/α-Fe(Co) + $Nd_2Fe_{14}B$/α-Fe multiphase nanohybrid magnet features a high high-temperature application potential. Moreover, this work gives a method of further improving the thermal stability of multiphase nanohybrid magnets.

Funding The study was financially supported by the Natural Science Foundation of Hebei province (No. E2021402001), project of Department of Education of Hebei Province (No. QN2019040), and the Science and Technology Research and Development Projects of Handan City (21422111275, 19422111008–20).

References

1. Gutfleisch, O., Willard, M.A., Brück, E., Chen, C.H., Sankar, S.G., Liu, J.P.: Magnetic materials and devices for the 21st century: stronger, lighter, and more energy efficient. Adv. Mater. **23**, 821–842 (2011)
2. Fingers, R.T., Rubertus, C.S.: Application of high temperature magnetic materials. IEEE Trans. Magn. **36**, 3373–3375 (2000)
3. Rong, C.B., Poudyal, N., Liu, X.B., Zhang, Y., Kramer, M.J., Liu, J.P.: High temperature magnetic properties of $SmCo_5$/α-Fe(Co) bulk nanocomposite magnets. Appl. Phys. Lett. **101**, 152401 (2012)
4. Kaplesh, K.: $RETM_5$ and RE_2TM_{17} permanent magnets development. J. Appl. Phys. **63**, R13–R57 (1988)
5. Sugimoto, S.: Current status and recent topics of rare-earth permanent magnets. J. Phys. Appl. Phys. **44**, 064001 (2011)
6. Pathak, A.K., Khan, M., Gschneidner, K.A., Jr., McCallum, R.W., Zhou, L., Sun, K., Dennis, K.W., Zhou, C., Pinkerton, F.E., Kramer, M.J., Pecharsky, V.K.: Cerium: an unlikely replacement of dysprosium in high performance Nd–Fe–B permanent magnets. Adv. Mater. **27**, 2663–2667 (2015)
7. Tenaud, Ph., Lemaire, H., Vial, F.: Recent improvements in NdFeB sintered magnets. J. Magn. Magn. Mater. **101**, 328–332 (1986)
8. Bauer, D., Diamond, D., Li, J., Sandalow, D., Telleen, P., Wanner, B.: Critical materials strategy. Technical Report, U.S. Department of Energy (DOE) 14–53 (2010)
9. Liu, S.: Recent developments in high-temperature permanent magnet materials. In: Liu, Y., Sellmyer, D.J., Shindo, D. (eds.) Handbook of Advanced Magnetic Materials, pp. 1329–1377. Springer, Boston, MA (2006)
10. Sagawa, M., Fujimura, S., Yamamoto, H., Matsuura, Y.: Permanent magnet materials based on the rare earth-iron-boron tetragonal compounds. IEEE Trans. Magn. **20**, 1584–1589 (1984)
11. Trench, A., Sykes, J.P.: Rare earth permanent magnets and their place in the future economy. Engineering **6**(2), 115–118 (2020)
12. Yue, M., Zhang, X.Y., Liu, J.P.: Fabrication of bulk nanostructured permanent magnets with high energy density: challenges and approaches. Nanoscale **9**, 3674–3697 (2017)
13. Jones, N.: The pull of stronger magnets. Nature **472**, 22–23 (2011)
14. Sellmyer, D.J.: Strong magnets by self-assembly. Nature **420**, 374–375 (2002)
15. Zhang, G., Shan, W., Guo, D.: Phase and grain size dependence of the pinning strength of nanocomposite magnets. J Supercond. Nov. Magn. **32**(6), 1599–1603 (2019)
16. Li, X., Lou, L., Song, W., Zhang, Q., Huang, G., Hua, Y., Zhang, H., Xiao, J., Wen, B., Zhang, X.: Controllably manipulating three-dimensional hybrid nanostructures for bulk nanocomposites with large energy products. Nano Lett. **17**, 2985–2993 (2017)
17. Huang, G., Li, X., Lou, L., Hua, Y., Zhu, G., Li, M., Zhang, H., Xiao, J., Wen, B., Yue, M., Zhang, X.: Engineering bulk, layered, multicomponent nanostructures with high energy density. Small **14**, 1800619 (2018)
18. Li, X., Lou, L., Song, W., Huang, G., Hou, F., Zhang, Q., Zhang, H., Xiao, J., Wen, B., Zhang, X.: Novel bimorphological anisotropic bulk nanocomposite materials with high energy products. Adv. Mater. **29**, 1606430 (2017)
19. Lou, L., Li, Y., Li, Xi., Li, H., Li, W., Hua, Y., Xia, W., Zhao, Z., Zhang, H., Yue, M., Zhang, X.: Directional magnetization reversal enables ultrahigh energy density in gradient nanostructures, Adv. Mater. **33**, 2102800 (2021)

20. Li, H., Li, X., Guo, D., Lou, L., Li, W., Zhang, X.: Three-dimensional self-assembly of core/shell-like nanostructures for high-performance nanocomposite permanent magnets. Nano Lett. **16**, 5631–5638 (2016)
21. Li, W., Li, L., Nan, Y. , Li, X., Zhang, X., Gunderov, D., Stolyarov, V., Popov, A.: Controllable nanocrystallization in amorphous $Nd_9Fe_{85}B_6$ via combined application of severe plastic deformation and thermal annealing, Appl. Phys. Lett. **91**, 062509 (2007)
22. Huang, G., Hou, F., Lou, L., Zhang, G., Li, M., Wei, B., Song, W., Zhang, Q., Huang, H., Li, X.: Bulk anisotropic multiphase nanohybrid magnets fabricated from compound precursors. J. Alloys Compd. **771**, 209–214 (2019)
23. Wang, S., Hung, N., Tian, H., Shafifiqul, I., Saito, R.: Switching behavior of a heterostructure based on periodically doped graphene nanoribbon. Phy. Rev. Appl. **16**(2), 024030 (2021)
24. Liu, J., Zhang, Y., Dimitrov, D., Hadjipanayis, G.: Microstructure and high temperature magnetic properties of Sm (Co,Cu,Fe,Zr)z (z= 6.7–9.1) permanent magnets. J. Appl. Phys. **85**, 2800–2804 (1999)
25. Liu, S.: Sm–Co high-temperature permanent magnet materials. Chin. Phys. B **28**, 017501 (2019)
26. Zhang, X.: Heterostructures: new opportunities for functional materials. Mater Res Lett. **8**(2), 49–59 (2020)
27. Liu, Y., Xu, L., Wang, Q., Li, W, Zhang X.: Development of crystal texture in Nd-lean amorphous $Nd_9Fe_{85}B_6$ under hot deformation. Appl. Phys. Lett. **94**(17), 172502 (2009)
28. Hou, F., Li, X., Zhang, G., Hua, Y., Li, M., Lou, L., Huang, G., Li, W., Zhang, X.: Fabrication of bulk anisotropic $Nd_2Fe_{14}B$/α-Fe nanocomposite magnets with two-step high-pressure thermal compression. J. Alloys Comp. **764**, 718–723 (2018)
29. Li, H., Lou, L., Hou, F., Guo, D., Li, W., Li, X., Gunderov, D., Sato, K., Zhang, X.: Simultaneously increasing the magnetization and coercivity of bulk nanocomposite magnets via severe plastic deformation. Appl. Phys. Lett. **103**(14), 142406 (2013)
30. Cui, W., Ma, L., Sepehri-Amin, H., Takahashi, Y., Hono, K.: The inflfluence of grain morphology and easy axis orientation on the coercivity of $Sm(Co_{0.9}Cu_{0.1})_5$ thin films. Acta Mater. **107**, 49–58 (2016)
31. Cui, W., Sepehri-Amin, H., Takahashi, Y., Hono, K.: Hard magnetic properties of spacer-layer-tuned NdFeB/Ta/Fe nanocomposite films. Acta Mater. **84**, 405–412 (2015)
32. Song, W., Li, X., Lou, L., Hua, Y., Zhang, Q., Huang, G., Zhang, X.: Anisotropic bulk $SmCo_7$ nanocrystalline magnets with high energy product. APL Mater. **5**(11), 116101 (2017)
33. Qiu, L., Zhao, L., Weng, X., Shen, L., Zhao, G., Wang, F., Xie, L.: A hybrid coercivity mechanism for exchange-coupled nanocomposite permanent magnets. J Rare Earths. **37**(10), 1030–1033 (2019)
34. Zhao, G., Zhao, L., Shen, L., Zhou, J., Qiu, L.: Coercivity mechanisms in nanostructured permanent magnets. Chin. Phys. B. **28**(7), 077505 (2019)
35. Walmer, M., Chen, C., Walmer, M.: A new class of Sm-TM magnets for operating temperatures up to 550 °C. IEEE Trans. Magn. **36**, 3376–3381 (2000)
36. Huang, G., Zhu, G., Lou, L., Yan, J., Song, W.P., Hou, F., Hua, Y., Zhang, Q., Li, X., Zhang, X.: Anisotropic bulk $Nd_2Fe_{14}B$/a-Fe nanohybrid magnets with an enhanced energy product. Mater. Lett. **217**, 219–222 (2018)
37. Lewis, L., Gallagher, K., Panchanathan, V.: The effect of Nb additions on the thermal stability of melt-spun $Nd_2Fe_{14}B$. J. Appl. Phys. **85**(8), 5926–5928 (1999)
38. Leonowicz, M., Spyra, M., Jezierska, E.: Improvement of the properties of hard magnetic NdFeB/Fe nanocomposites by minor addition of refractory metals. Mech. Adv. Mater. Struc. **18**(3), 181–184 (2011)
39. Cui, W., Takahashi, Y., Hono, K.: $Nd_2Fe_{14}B$/FeCo anisotropic nanocomposite films with a large maximum energy product. Adv Mater. **24**(48), 6530–6535 (2012)
40. Zhang, X., Guan, Y., Zhang, J.: Study of interface structure of α-Fe/$Nd_2Fe_{14}B$ nanocomposite magnets. Appl. Phys. Lett. **80**(11), 1966–1968 (2002)
41. Zhang, X., Guan, Y., Zhang, J., Sprengel, W., Reichle, K., Blaurock, K., Reimann, K., Schaefer, H-E.: Evolution of interface structure of nanocomposites prepared by crystallization from the amorphous alloy. Phys. Rev. B **66**(21), 212103 (2002)